

Simulation and improvement of land surface processes in Nameqie, Central Tibetan Plateau, using the Community Land Model (CLM3.5)

Xuejia Wang · Meixue Yang · Guojin Pang ·
Guoning Wan · Xiaolei Chen

Received: 12 May 2014 / Accepted: 19 November 2014 / Published online: 3 December 2014
© Springer-Verlag Berlin Heidelberg 2014

Abstract Accurate simulation of thermal and hydrological soil processes is highly important for studying cold region climates. In this paper, two thermal conductivity parameterization schemes for soil proposed by Johansen and Luo were combined with a groundwater parameterization scheme (JN and LN schemes) to modify the soil water and heat parameterization schemes in the Community Land Model (CLM3.5). Land surface processes in the Central Tibetan Plateau were simulated based on the original scheme (Farouki scheme), JN scheme, and LN scheme using the atmospheric forces from meteorological observations at Nameqie, and they were compared with observed data in the same period. We found that all three schemes underestimated the upward shortwave radiation and overestimated the upward longwave radiation and net

radiation, but the predictions from the modified scheme better agreed with the observations. The three schemes simulated the average soil temperatures higher than the observation data. The modified schemes, particularly the LN scheme, resulted in better predictions of the soil temperature compared with the original CLM3.5. More thawing days were simulated by three schemes. The observed freezing and thawing proceeded from the upper layers to the lower layers; however, the frozen soil in the Farouki and LN schemes began to thaw in the upper layers and below ~160 cm. The differences in the simulated soil thermal conductivity among the three schemes increased with depth. The soil thermal conductivity simulated by the Farouki scheme was the highest, while the smallest values were generated by the JN scheme. The soil volumetric water content of the Farouki scheme below a 100 cm depth was obviously larger than the observed data. After considering water exchange between the soil column and its underlying aquifer, the JN scheme and, particularly, the LN scheme, simulated the soil volumetric water content slightly higher than but similarly to the observed data.

X. Wang · M. Yang (✉) · G. Wan
State Key Laboratory of Cryospheric Sciences, Cold and Arid Regions Environmental and Engineering Research Institute, Chinese Academy of Sciences, Lanzhou 730000, Gansu, China
e-mail: mxyang@lzb.ac.cn

X. Wang
e-mail: wangxuejia86@163.com

X. Wang · X. Chen
University of Chinese Academy of Sciences,
Beijing 100049, China

G. Pang
Laboratory of Remote Sensing and Geospatial Science, Cold and Arid Regions Environmental and Engineering Research Institute, Chinese Academy of Sciences, Lanzhou 730000, Gansu, China

X. Chen
State Key Laboratory of Numerical Modeling for Atmospheric Sciences and Geophysical Fluid Dynamics, Institute of Atmospheric Physics, Chinese Academy of Sciences, Beijing 100029, China

Keywords Community Land Model · Land surface process · Soil thermal conductivity · Soil temperature · Freeze/thaw · Soil volumetric water content

Introduction

Because of its particular geographical location and complex underlying surfaces, the Tibetan Plateau has a tremendous impact on its surroundings and the global climate and environment (Rangarajan 1963; Ye and Gao 1979; Xu et al. 2008; Yang et al. 2010, 2014; Yao et al. 2012; Wu et al. 2012). Permafrost is a product of cold climatic

conditions and is widespread in high-latitude and high-elevation regions (Zhang et al. 2007a). Permafrost and seasonal frozen ground are extensive in the Tibetan Plateau, and their seasonal freezing and thawing processes and spatial distributions lead to variations in the surface moisture conditions and energy balance. These features may even influence precipitation and atmospheric circulation in East Asia (Wang et al. 2003; Yang et al. 2003, 2007; Guo et al. 2010). Since the 1970s, international scientists have been committed to conducting continuous field observations, including the first Tibetan Plateau meteorological research in 1979, the Global Energy and Water Cycle Experiment/Asian Monsoon Experiment on the Tibetan Plateau (GAME-Tibet, 1996–2000), and the Coordinated Enhanced Observing Period/Asia–Australia Monsoon Project on the Tibetan Plateau (CAMP-Tibet, 2001–2005), which were successively and jointly conducted by Chinese and Japanese scientists. Several subsequent field campaigns and hydro-meteorological observations were also conducted (Yang et al. 2014). Accordingly, abundant firsthand field data were acquired. These experiments have greatly improved the level of awareness and understanding of the interactions between the land surface and atmosphere in the Tibetan Plateau (cf., Ma et al. 2009 and references therein).

Recently, the use of land surface models to investigate soil freezing and thawing processes and land-atmosphere interactions has become an indispensable tool. It was widely recognized that the simulated accuracy of land models for land surface processes directly affects the results of the climate model. Studies on parameterization schemes for soil freezing and thawing processes in land surface models and climate models suggest that ignoring these processes will result in conspicuous underestimates or overestimates of soil temperature and liquid water content, frozen depth, and energy fluxes when the soil is frozen (e.g., Peters-Lidard et al. 1998; Koren et al. 1999; Li and Koike 2003). Fortunately, soil freezing and thawing parameterization schemes for land surface models have been developed. However, descriptions of the soil freezing and thawing processes in some well-known land surface models are different in detail. Li and Koike (2003) grouped the descriptions of frozen soil processes in land surface models into three categories: the first category provides simple descriptions of the hydraulic and thermal properties of frozen soil, such as SSIB, SiB2 (Sellers et al. 1986, 1996) and BATS (Dickinson et al. 1993); the second category, i.e., the Best Approximation of Surface Exchanges (BASE) (Slater et al. 1998) and the CCSR/NIES GCM (Takata and Kimoto 2000), determines ice production rates that depend on the amount of heat energy available for phase change processes; the third category, e.g., the Mesoscale Analysis and Prediction System (MAPS)

(Smirnova et al. 2000), the Variable Infiltration Capacity (VIC) model (Cherkauer and Lettenmaier 1999), and the mesoscale Eta model (Koren et al. 1999), calculates maximum unfrozen water content using soil matric potential when the soil temperature is below the freezing point.

Recent studies indicated that describing land surface processes, particularly soil freezing and thawing processes in the Tibetan Plateau, have not been well represented in land surface models and that further improvement work is needed (Yang et al. 2009; Wang et al. 2013). Although some improvement in soil water–heat parameterization schemes has been made in the Tibetan Plateau (e.g., Zhang and Lü 2002; Zhang et al. 2007b; Luo et al. 2009a; Xiao et al. 2012; Yi et al. 2013), the near-absence of high-quality, continuous and valid observations precludes the simulation and improvement of soil conditions. The Community Land Model (CLM) has been applied in the Tibetan Plateau (e.g., Xia et al. 2011; Guo and Wang 2013; Chen et al. 2013a, b; Wang et al. 2013) and has been coupled to global and regional climate models (such as CAM, CCSM, COSMO, and RegCM) to study interannual and interdecadal variability, paleoclimate regimes, and projections of future climate change (Collins et al. 2006; Rockel et al. 2008; Davin et al. 2011; Xu and Dirmeyer 2011; Giorgi et al. 2012; Wang et al. 2013). However, until now, achievements based on a series of field observations have not yet been incorporated into the state-of-the-art and widely used Community Land Model (CLM). There are large gaps between field observations and land surface process modeling.

Luo et al. (2009b) retained the calculations from Farouki's soil thermal conductivity (1981) in the Common Land Model (CoLM) and added the soil thermal conductivity schemes of Johansen (1977) and Côté and Konrad (2005) to modify the thermal conductivity schemes of soil solids and dry soil. The authors eventually included Kersten's number scheme according to field-observed soil textures and thermal conductivities based on soil surveys and sampling in the Central Tibetan Plateau. The interaction between groundwater and soil moisture relies on the exchange of water between unsaturated soil and its underlying aquifer via gravity and capillary forces. Groundwater dynamics also control runoff generation, which can further affect the computation of soil moisture and evapotranspiration in a climate model (Niu et al. 2007). Niu et al. (2007, 2011) modified a groundwater model (SIMGM) to explain the exchanges of water between soil columns and their underlying aquifers. For these reasons, considering the coupling and interaction between soil temperature and soil water content, we first used Johansen's thermal conductivity scheme to modify the original soil thermal conductivity scheme of Farouki; then, we modified a groundwater model according to the work of

Niu et al. (hereafter referred to as the JN scheme). We similarly used the schemes of Luo et al. and Niu et al. (the LN scheme) to modify the original soil water–heat parameterization schemes. In this paper, observational data and simulated land surface processes from the original soil water–heat parameterization schemes (the Farouki scheme), the JN scheme and the LN scheme were compared at NMQ in the Central Tibetan Plateau to investigate the effects of different water–heat parameterization schemes on land surface process simulations and to identify an appropriate water–heat parameterization scheme for the Central Tibetan Plateau.

Model descriptions

Community Land Model (CLM3.5)

CLM3.5 incorporates the advantages of the Biosphere–Atmosphere Transfer Scheme (BATS), Institute of Atmospheric Physics, the Chinese Academy of Sciences land model (IAP94), and the NCAR LSM, and it is an upgrade of CLM3.0. The land surface in CLM3.0 is represented by several plant functional types (PFTs) with different biological and hydrological characteristics and by soil texture types that determine the thermal and hydrological properties of the soil. Biophysical processes simulated by CLM3.0 include solar and longwave radiation interactions with the vegetation canopy and soil, momentum and turbulent fluxes from the canopy and soil, heat transfer in soil and snow, the hydrology of the canopy, soil, and snow, and stomatal physiology and photosynthesis. A detailed description of how these processes are parameterized in CLM3.0 is provided by Oleson et al. (2004). Compared with CLM3.0, the modifications in CLM3.5 are as follows: new surface datasets and parameterizations, such as surface datasets based on Moderate Resolution Imaging Spectroradiometer (MODIS) products (Lawrence and Chase 2007); improved canopy integration scheme (Thornton and Zimmermann 2007); a simple TOPMODEL-based model for surface and subsurface runoff (Niu et al. 2005); water-table depth determination by a simple groundwater model (Niu et al. 2007); and the concept of supercooled soil water through the implementation of a freezing-point depression equation and the relaxed dependence of hydraulic properties on the soil-ice content through incorporating the fractional impermeable area to modify the frozen soil scheme (Niu and Yang 2006). Spatial land-surface heterogeneity in CLM is represented as a nested subgrid hierarchy in which grid cells are composed of multiple land units, snow/soil columns, and PFTs. The profile of CLM3.5 is represented by 10 uneven layers of soil and up to five layers of snow,

depending on the snow depth. The soil and snow temperature are solved based on the thermal conductivity equation (Oleson et al. 2004).

Soil thermal conductivity parameterization schemes

Farouki scheme

The soil thermal conductivity parameterization scheme in CLM3.5 is Farouki’s scheme (Farouki 1981; Oleson et al. 2013), which is one of the most frequently and widely used schemes.

Soil thermal conductivity λ_i ($\text{W m}^{-1} \text{K}^{-1}$) is expressed as:

$$\lambda_i = \begin{cases} K_{e,i}\lambda_{\text{sat},i} + (1 - K_{e,i})\lambda_{\text{dry},i}, & S_{r,i} \geq 1 \times 10^{-7} \\ \lambda_{\text{dry},i}, & S_{r,i} < 1 \times 10^{-7} \end{cases} \quad (1)$$

where $\lambda_{\text{sat},i}$ is the saturated soil thermal conductivity, $\lambda_{\text{dry},i}$ is the dry soil thermal conductivity, $K_{e,i}$ is the Kersten number, $S_{r,i}$ is the degree of saturation, and i is the soil layer.

The saturated soil thermal conductivity $\lambda_{\text{sat},i}$ ($\text{W m}^{-1} \text{K}^{-1}$) depends on the thermal conductivities of soil solids, liquid water and ice.

$$\lambda_{\text{sat},i} = \begin{cases} \lambda_{s,i}^{1-\theta_{\text{sat},i}} \lambda_{\text{liq},i}^{\theta_{\text{sat},i}}, & T_i \geq T_f \\ \lambda_{s,i}^{1-\theta_{\text{sat},i}} \lambda_{\text{liq},i}^{\frac{\theta_{\text{liq},i}}{\theta_{\text{liq},i} + \theta_{\text{ice},i}} \theta_{\text{sat},i}} \lambda_{\text{ice},i}^{\theta_{\text{sat},i} \left(1 - \frac{\theta_{\text{liq},i}}{\theta_{\text{liq},i} + \theta_{\text{ice},i}}\right)}, & T_i < T_f \end{cases} \quad (2)$$

where T_f is the freezing point, $\theta_{\text{sat},i}$ is the soil saturated water content, $\theta_{\text{liq},i}$ is the soil liquid water content, and $\lambda_{\text{liq},i}$ and $\lambda_{\text{ice},i}$ are the thermal conductivities of water ($0.57 \text{ W m}^{-1} \text{K}^{-1}$) and ice ($2.29 \text{ W m}^{-1} \text{K}^{-1}$), respectively. The thermal conductivity of soil solids $\lambda_{s,i}$ varies with the sand and clay content.

$$\lambda_{s,i} = \frac{8.80 (\% \text{ sand})_i + 2.92 (\% \text{ clay})_i}{(\% \text{ sand})_i + (\% \text{ clay})_i} \quad (3)$$

where $(\% \text{ sand})_i$ and $(\% \text{ clay})_i$ are the percent compositions of the sand and clay in each soil layer.

Dry soil thermal conductivity $\lambda_{\text{dry},i}$ is a function of dry soil density $\rho_{d,i}$.

$$\lambda_{\text{dry},i} = \frac{0.135 \rho_{d,i} + 64.7}{2700 - 0.947 \rho_{d,i}} \quad (4)$$

Kersten’s number $K_{e,i}$ is only a function of the degree of saturation $S_{r,i}$ and the phase of the water.

$$K_{e,i} = \begin{cases} \log(S_{r,i}) + 1 \geq 0 & T_i \geq T_f \\ S_{r,i} & T_i < T_f \end{cases} \quad (5)$$

where the degree of saturation ($S_{r,i}$) is

$$S_{r,i} = \left(\frac{\theta_{\text{liq},i} + \theta_{\text{ice},i}}{\theta_{\text{sat},i}} \right) \leq 1 \quad (6)$$

Johansen scheme

The soil thermal conductivity scheme of Johansen (1977) is similar to that of Farouki. The only differences between the schemes are the calculations of the soil solids' thermal conductivity and Kersten number. The soil solids' thermal conductivity k_s of Johansen is given as

$$k_s = k_q^q k_o^{1-q} \quad (7)$$

where the thermal conductivity of quartz is $k_q = 7.7 \text{ W m}^{-1} \text{ K}^{-1}$, the thermal conductivity of other minerals is $k_o = 2.0 \text{ W m}^{-1} \text{ K}^{-1}$, and q is the quartz content in the soil (0.5 times the sand content).

For unfrozen soils,

$$K_e = \begin{cases} 0.7 \lg S_r + 1.0, & S_r > 0.5 \\ \lg S_r + 1.0, & S_r > 0.1 \end{cases} \quad (8)$$

$$\text{For frozen soils, } K_e = S_r \quad (9)$$

Luo scheme

Luo et al. (2009b) retained Farouki's formula for soil thermal conductivity, replaced the soil solids and dry soil thermal conductivity schemes with those of Johansen (1977) and Côté and Konrad (2005), and modified the parameters related to Kersten's number based on field soil investigations and sampling. The detailed scheme is shown as follows:

$$\lambda_i = \begin{cases} K_{e,i} \lambda_{\text{sat},i} + (1 - K_{e,i}) \lambda_{\text{dry},i}, & S_{r,i} \geq 1 \times 10^{-5} \\ \lambda_{\text{dry},i}, & S_{r,i} < 1 \times 10^{-5} \end{cases} \quad (10)$$

$$\lambda_{\text{sat},i} = \begin{cases} \lambda_{s,i}^{1-\theta_{\text{sat},i}} \lambda_{\text{liq},i}^{\theta_{\text{sat},i}}, & T_i \geq T_f \\ \lambda_{s,i}^{1-\theta_{\text{sat},i}} \lambda_{\text{liq},i}^{\theta_{\text{liq},i} + \theta_{\text{ice},i}} \lambda_{\text{ice},i}^{\theta_{\text{sat},i}} \left(1 - \frac{\theta_{\text{liq},i}}{\theta_{\text{liq},i} + \theta_{\text{ice},i}} \right), & T_i < T_f \end{cases} \quad (11)$$

$$\lambda_{\text{dry},i} = \chi \times 10^{-\eta \theta_{\text{sat},i}} \quad (12)$$

where χ ($\text{W m}^{-1} \text{ K}^{-1}$) and η (unitless) are parameters that account for the particle shape effect. Luo et al. (2009b) provided χ and η values for sand, clay and other mixed soil texture types. The fine mineral-mixed dry soil thermal conductivity $\lambda_{\text{dry},m}$ of each layer is:

$$\lambda_{\text{dry},m} = \lambda_{\text{dry},\text{sand}} f_{\text{sand}} + \lambda_{\text{dry},\text{clay}} f_{\text{clay}} + \lambda_{\text{dry},\text{other}} f_{\text{other}} \quad (13)$$

where $\lambda_{\text{dry},\text{sand}}$, $\lambda_{\text{dry},\text{clay}}$ and $\lambda_{\text{dry},\text{other}}$ are the dry thermal conductivities of sand, clay and other mixed soil, respectively. f_{sand} , f_{clay} and f_{other} are the volumetric fractions of sand, clay and other mixed soil, respectively.

The Kersten number of each layer is given as

$$K_e = \frac{\kappa S_r}{1 + (\kappa - 1) S_r} \quad (14)$$

where κ is the empirical parameter used to account for different soil texture types. Values have been assigned for both frozen and unfrozen states and for sand, clay and other mixed soil texture types. For mixed soil, the Kersten number $K_{e,m}$ is:

$$K_{e,m} = K_{e,\text{sand}} f_{\text{sand}} + K_{e,\text{clay}} f_{\text{clay}} + K_{e,\text{other}} f_{\text{other}} \quad (15)$$

where $K_{e,\text{sand}}$, $K_{e,\text{clay}}$ and $K_{e,\text{other}}$ are the Kersten numbers of sand, clay and other mixed soil texture types of each layer, respectively.

Groundwater model (SIMGM)

An aquifer is often defined as the geological structure that constitutes soil, gravel, and/or permeable rock where groundwater resides. Niu et al. (2007) defined an "aquifer" as the area below the model soil columns. The temporal variation in the water stored in an unconfined aquifer, W_a (mm), is expressed as:

$$\frac{dW_a}{dt} = Q - R_{sb} \quad (16)$$

where Q (mm s^{-1}) is the recharge to the aquifer, R_{sb} (mm s^{-1}) is the discharge from the aquifer (base flow or subsurface runoff). Then, Q is parameterized following Darcy's law and is positive when water enters the aquifer:

$$Q = -K_\alpha \frac{-z_\nabla - (\psi_{\text{bot}} - z_{\text{bot}})}{z_\nabla - z_{\text{bot}}} \quad (17)$$

where K_α is the hydraulic conductivity of the aquifer ($\text{kg m}^{-2} \text{ s}^{-1}$), z_∇ is the water-table depth (m), and $z_{\text{bot}} = 2.98 \text{ m}$ is the node depth of the bottom layer. The matric potential of the bottom layer (mm) ψ_{bot} is defined as:

$$\psi_{\text{bot}} = \psi_{\text{sat},\text{bot}} (\theta_{\text{liq},\text{bot}} / \theta_{\text{sat},\text{bot}})^{-b} \quad (18)$$

$\psi_{\text{sat},\text{bot}}$ and b are the saturated soil matric potential (mm) and soil-texture-dependent Clapp and Hornberger (1978) exponents, respectively.

The above descriptions are only applicable to the case when the groundwater level is lower than the depth of the bottom layer (3.43 m). When the water table is within the soil column, there is no exchange of water between the soil column and the aquifer. Therefore, Niu et al. (2007, 2011) revised the recharge rate Q_i as:

$$Q_i = -K_{i,\nabla} \frac{(\psi_{\text{sat}} - z_\nabla) - (f_{\text{mic}} \psi_i - z_i)}{z_\nabla - z_i} \quad (19)$$

where $K_{i,\nabla}$ is the hydraulic conductivity between layer i and the water table, and ψ_i and z_i are the matric potential and the node depth of the i th layer, respectively. f_{mic} is

introduced as the fraction of micropore content in the bottom layer soil to limit the upward flow (depending on the level of structural soil), ranging from 0.0 to 1.0. $f_{mic} = 0.0$ indicates structural soil or aquifers without micropores, while $f_{mic} = 1.0$ indicates textural soil full of micropores. A larger f_{mic} produces wetter soil with less soil moisture variability. Here, it is set to 0.5.

The subsurface runoff or discharge, R_{sb} ($\text{kg m}^{-2} \text{s}^{-1}$), is expressed as (Niu et al. 2005):

$$R_{sb} = (1 - F_{frz})R_{sb,max}e^{-f(z_{\nabla})} \quad (20)$$

Then, it is modified as (Niu et al. 2007):

$$R_{sb} = (1 - F_{frz})R_{sb,max}e^{-f(z_{\nabla}-z)} \quad (21)$$

where $R_{sb,max} = 4.5 \times 10^{-4}$ is the maximum subsurface runoff when the grid-averaged water-table depth is zero.

The fractional saturated area F_{sat} is parameterized as (Niu et al. 2007):

$$F_{sat} = (1 - F_{frz})F_{max}e^{0.5fz_{\nabla}} + F_{frz} \quad (22)$$

where F_{max} is the potential or maximum saturated fraction of a GCM grid cell. $f (=0.4)$ is the runoff decay factor. F_{frz} is the fractional impermeable area determined by the soil-ice content in the surface layer (Niu and Yang 2006).

The fractional saturated area F_{sat} is expressed as (Niu et al. 2011):

$$F_{sat} = (1 - F_{frz})F_{max}e^{0.5f(z_{\nabla}-z)} + F_{frz} \quad (23)$$

where z_{∇} is the water-table depth, and z is the depth of the soil layer.

Study area and parameter selection

The general conditions in the study area

Nameqie (NMQ) (31.51°N, 91.40°E; 4,590 m asl) is located in the Nameqie township of Naqu County in the Central Tibetan Plateau (Fig. 1a). The climate of the entire Naqu area is characterized by extreme cold, oxygen-deficient, and dry conditions. At NMQ, the mean wind speed was 3.39 m s^{-1} , the mean temperature was $0.24 \text{ }^{\circ}\text{C}$, and the annual precipitation was 519.7 mm in 2011. The surface is flat and open. The area mainly comprises sands, while fine gravels are sparsely distributed; a 4–5 cm alpine meadow is uneven distributed across the surface. The shallow soil layer is sandy loam, and the deep soil layer is sandy soil. At a 0–30 cm depth, within the vegetation root layer, the soil color is ash black. At that depth, the soil texture is sandy loam. At a 30–220 cm depth, the soil color is caesious, and the soil texture is coarse sand with a small amount of gravel.

Parameter selection and experiment design

Meteorological variables at the NMQ site, including air temperature, precipitation, soil temperature, soil water content, humidity, relative humidity, vapor pressure, radiation, wind direction, and wind speed, have been measured every 30 min since August 2010 (Fig. 1b). The depths of the soil temperature measurements are 4, 20, 40, 60, 80, 100, 130, 160, 200 and 220 cm; the depths of the soil water content measurements are 4, 20, 60, 100, 160 and 210 cm. The observation variables and instruments are listed in Table 1. The input data of the model mainly refer to the parameters of the 30-min atmospheric forcing data, vegetation index, and soil texture in the simulation by Chen et al. (2013b) using CLM3.0 at the NMQ site. The atmospheric forcing data were input according to Greenwich Mean Time. The soil column in the model is divided into 10 layers. From the surface to the deep layer node, the soil depth is 0.0071, 0.0280, 0.0623, 0.1189, 0.2122, 0.3661, 0.6189, 1.0380, 1.7276, and 2.8647 m. The soil textures in each layer are from 10 field-measured soil samples (4, 20, 40, 60, 80, 100, 130, 160, 200 and 220 cm) (Table 2). The leaf area and stem area index are from MODIS (Lawrence and Chase 2007). For a comparison with the observed data, the model-simulated soil temperature at each depth must be linearly interpolated. In the study, three groups of simulation experiments (the Farouki scheme, JN scheme, and LN scheme) were conducted with the same atmospheric forcing data, vegetation data, soil texture data, and simulation period (1 October 2010 to 31 May 2012). To eliminate the effect of the initial land surface conditions, such as the soil moisture memory, the first month (October 2010) was used for the model spin-up and excluded in the analysis.

Atmospheric forcing variables

The atmospheric forcing variables input into CLM3.5 were downward shortwave radiation, air temperature and precipitation, specific humidity, wind speed, and air pressure (Fig. 2). From the figure, the temperature, specific humidity, downward shortwave radiation and air pressure have obvious seasonal variations. Except for the wind speed, the variables are all high in summer and low in winter. The downward shortwave radiation has large seasonal variations; the amplitude in summer is larger than that in winter. The daily mean downward shortwave radiation is 247.51 W m^{-2} in the summer (May to September) of 2011 and 208.72 W m^{-2} in the winter (October to April). The air temperature from December to April of the next year is below $0 \text{ }^{\circ}\text{C}$. The annual range in the temperature is large ($26.92 \text{ }^{\circ}\text{C}$ in 2011). The precipitation is mainly concentrated in summer (June to August), as much

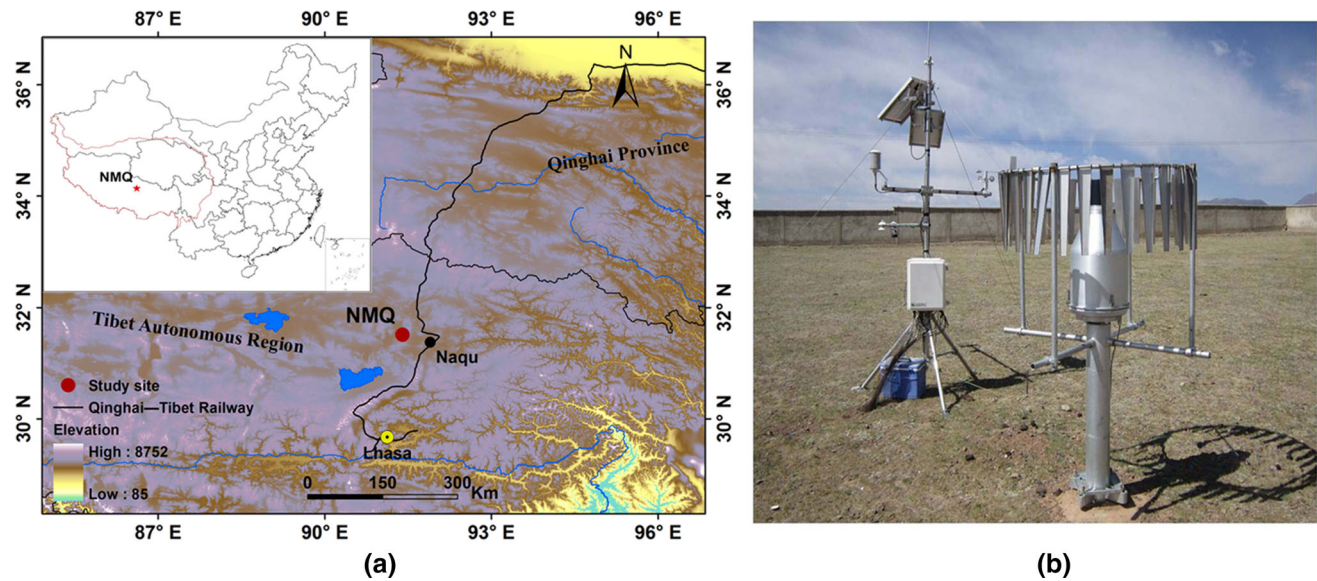


Fig. 1 Geographical location (a) and field photograph of the MNQ site (b)

Table 1 Specification of the measurements and the instruments

Observation element	Instrument and origin	Height (depth) (m)
Wind direction and wind speed	(034B, MetOne)	2
Snow depth	(SR50-A, Campbell)	1.36
Air temperature, relative humidity	(HMP-L, Vaisala)	2
Soil temperature	(109SS, Campbell)	0.04, 0.2, 0.4, 0.6, 0.8, 1.00, 1.30, 1.60, 2.00, 2.20
Soil water content	(CS616, Campbell)	0.04, 0.20, 0.60, 1.0, 1.6, 2.1
Precipitation	(T-200B, Geonor)	1.78
Radiation	(NR-01, Kipp&Zonen)	1.5
Pressure	(CS106, Delta Tankers)	2

as 64 % in 2011. The specific humidity is higher in summer than in winter. Thus, the climate is wet in summer but dry in winter. The wind speed is high in winter but low in summer. The amplitude of the daily wind variations is larger in winter than in summer. The change in the air pressure agrees with the temperature, showing that pressure is high in summer but low in winter.

Performance measures

The simulated results from the three schemes were compared with the observed data on the basis of three statistical analyses: the correlation coefficient (r), bias (Bias), and standard error of the estimate (SEE). The methods for calculating r , Bias, and SEE are as follows:

$$r = \frac{\sum_{i=1}^n (S_i - \bar{S})(O_i - \bar{O})}{\sqrt{\sum_{i=1}^n (S_i - \bar{S})^2} \sqrt{\sum_{i=1}^n (O_i - \bar{O})^2}} \quad (24)$$

$$\text{Bias} = \sum_{i=1}^n \frac{S_i - O_i}{n} \quad (25)$$

$$\text{SEE} = \sqrt{\frac{\sum_{i=1}^n (S_i - O_i)^2}{n - 2}} \quad (26)$$

where S_i is the simulation result, \bar{S} is the average simulation, O_i is the observation result, \bar{O} is the average observation, and n is the total number of data.

Results and analysis

Radiation components

Net radiation is the balance of four radiation components, or the summation of net shortwave radiation and net longwave radiation. Figure 3 shows the scatter plots of the Farouki scheme's simulated downward shortwave radiation, downward longwave radiation and net radiation

Table 2 Soil depth (thickness), soil texture, and soil solids’ thermal conductivity in 10 layers at NMQ

Layer	Soil depth (m)	Soil thickness (m)	Node depth (m)	Soil texture (%)		Farouki scheme ($W m^{-1} K^{-1}$)	Johansen scheme ($W m^{-1} K^{-1}$)
				Sand	Clay		
1	0.0175	0.0175	0.0071	74.88	5.03	8.43	3.31
2	0.0451	0.0276	0.028	74.88	5.03	8.43	3.31
3	0.0906	0.0455	0.0623	74.88	5.03	8.43	3.31
4	0.1656	0.075	0.1189	81.01	4.24	8.51	3.45
5	0.2891	0.1235	0.2122	83.21	3.11	8.59	3.50
6	0.493	0.2039	0.3661	85.27	10.32	8.17	3.55
7	0.8289	0.3359	0.6198	87.21	11.03	8.14	3.60
8	1.3828	0.5539	1.038	93.01	5.46	8.47	3.74
9	2.2961	0.9133	1.7276	94.42	1.26	8.72	3.78
10	3.4331	1.137	2.8647	95.21	1.02	8.74	3.80

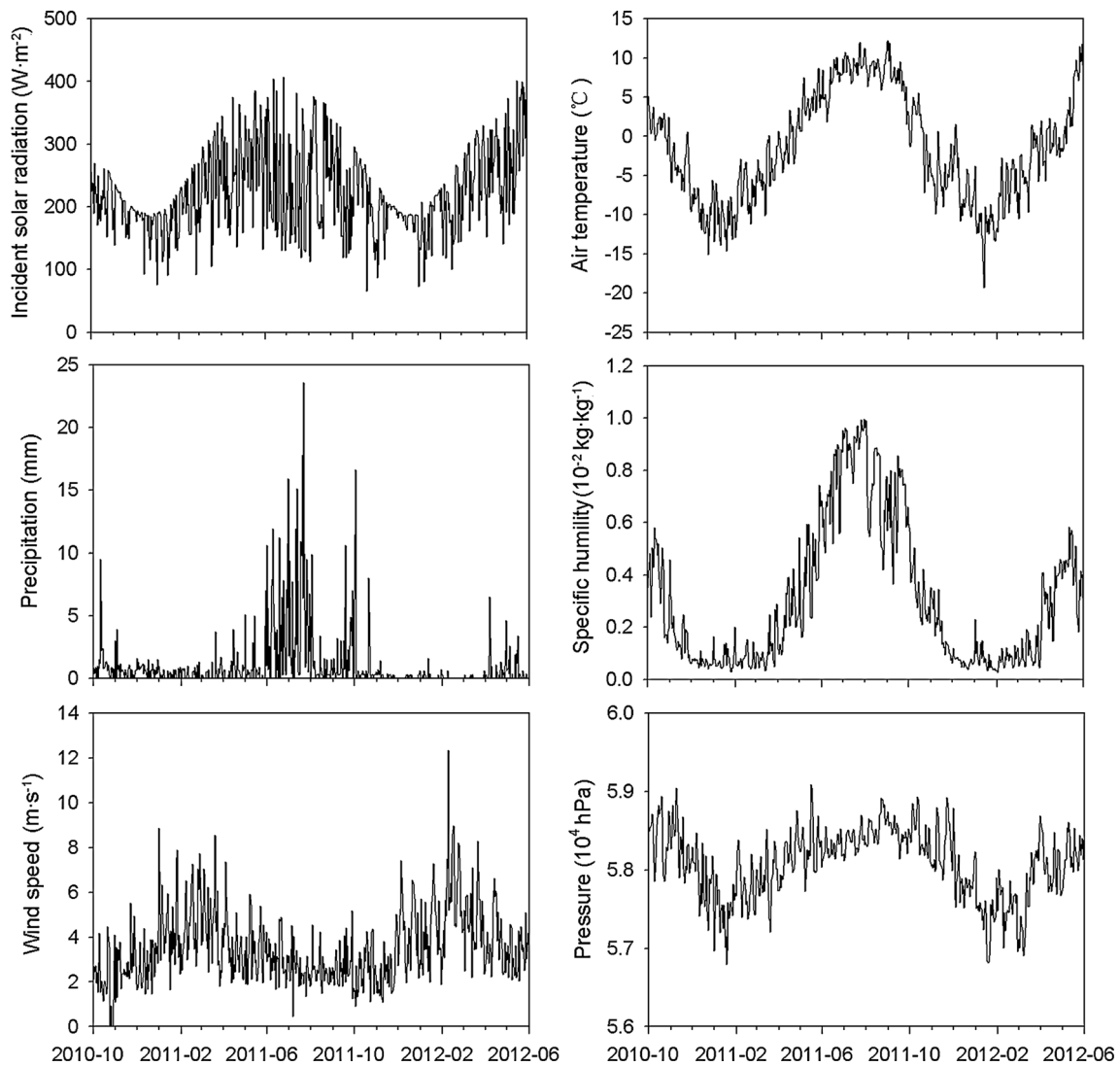


Fig. 2 Atmospheric forcing variables input into CLM3.5: downward shortwave radiation, air temperature and precipitation, specific humidity, wind speed, and air pressure

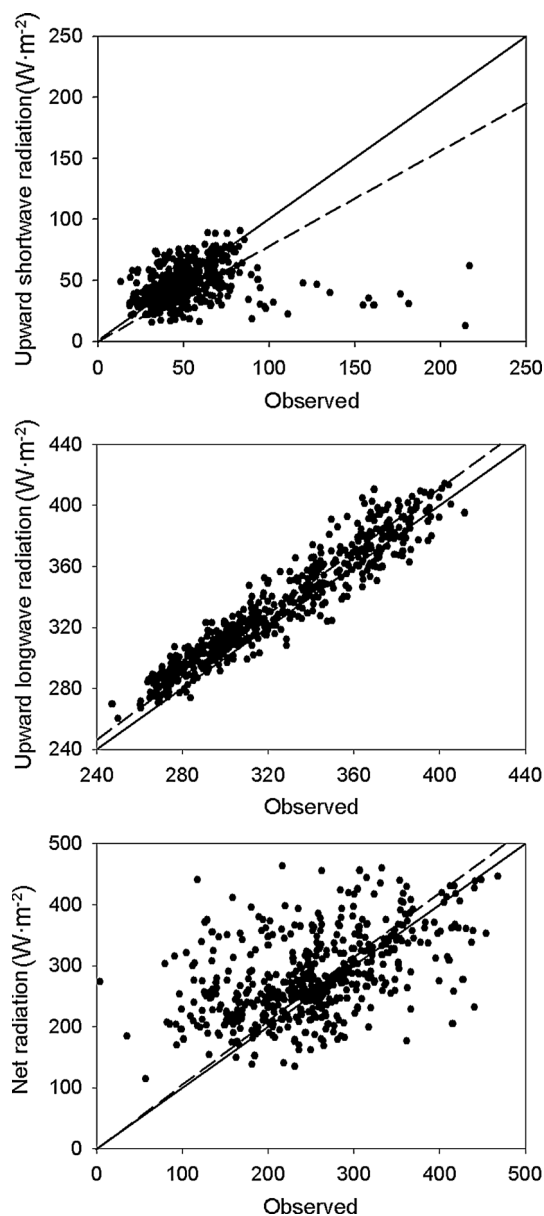


Fig. 3 Scatter plots of the daily mean upward shortwave radiation, upward longwave radiation, and net radiation (observations and Farouki scheme). The solid line 1:1; the dashed line regression

compared with the observational values (the slight difference between the JN and LN schemes' simulated radiation and the Farouki scheme's simulated radiation are not easily presented in the same figure, so they are omitted here). When the upward shortwave radiation is below 100 W m^{-2} , the simulated values are in good agreement with the observed values. However, in the high value area, the model-observation differences are large, i.e., the simulated values are small. This may be the result of error related to the precipitation (Luo et al. 2009a). The instrument that monitors precipitation records liquid water in winter, so solid precipitation is not completely accounted

for (i.e., the precipitation is underestimated). Therefore, less snow leads to a low surface albedo, which causes reduced upward shortwave radiation. On average, the upward shortwave radiation simulated by the Farouki scheme is 5.478 W m^{-2} lower than the observed value (Table 3). Although the correlation coefficients between the simulated upward shortwave radiation and observed values are low, they still exceeded the 99 % confidence level. Three schemes simulated upward longwave radiation very close to the observed values, and the correlation coefficients all reach 0.959. However, the schemes overestimate the upward longwave radiation by $8.523\text{--}9.272 \text{ W m}^{-2}$. The correlation coefficients between the simulated net radiation and observed values are all greater than 0.49, but the simulated values are overestimated by $25.74\text{--}26.59 \text{ W m}^{-2}$. Compared with the observed data, the JN scheme improves the radiation components. The correlation coefficients of the LN scheme increased, and the Bias and SEE (except for the upward longwave radiation) decreased when compared with the JN scheme.

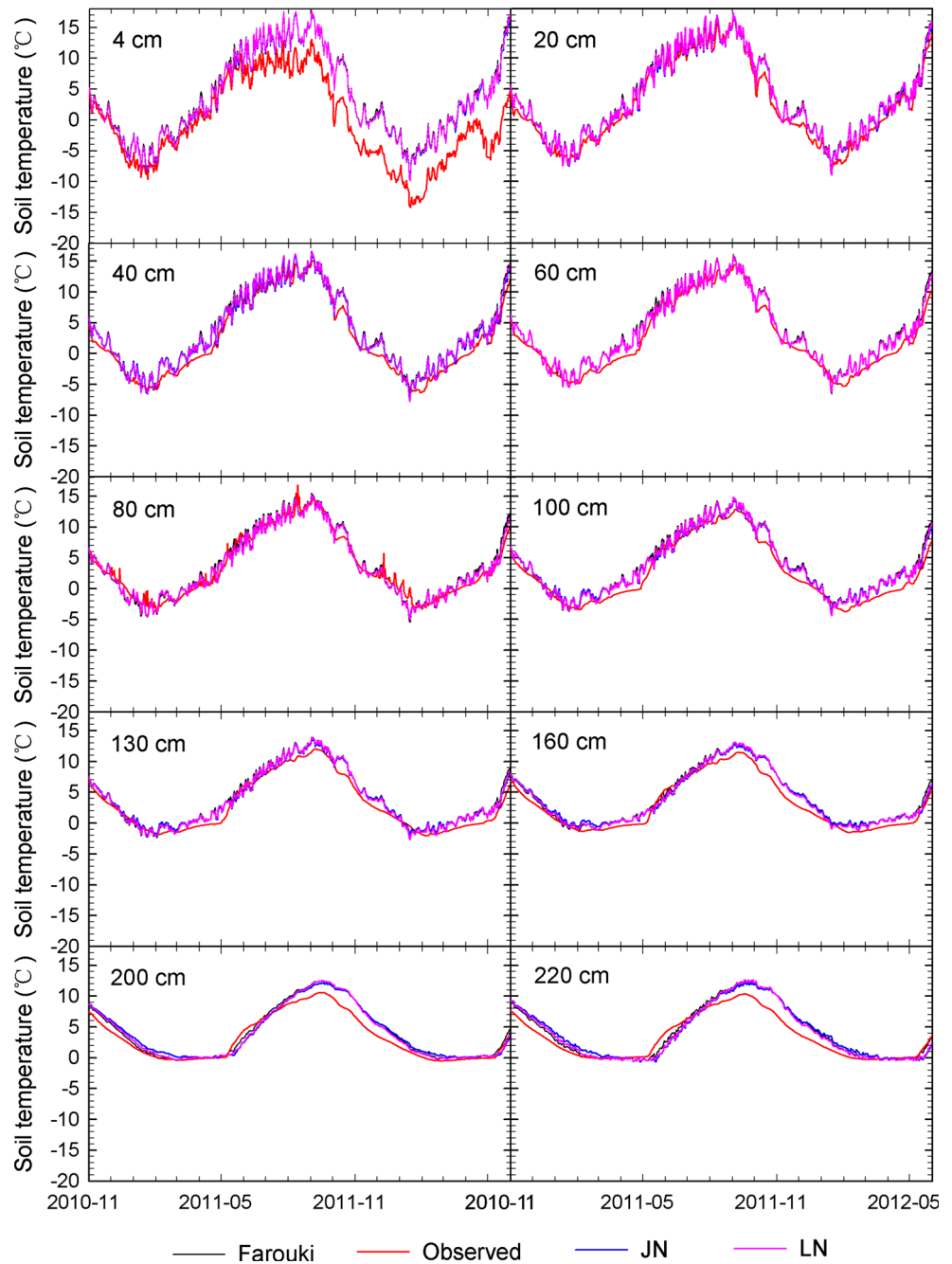
Soil temperature and freezing–thawing processes

Figure 4 displays the observed and simulated daily mean soil temperature over time at different depths. Three schemes are capable of providing good simulations of the evolution of the soil temperature. Because of the effect of the air temperature, the shallow soil layer temperatures greatly fluctuate. The effect of the air temperature on the soil temperature diminishes with depth. Therefore, the soil temperature curves gradually level off. The three schemes simulate the middle and lower soil layer temperatures well

Table 3 Statistical values of the three schemes' simulated and observed radiation components

	Upward shortwave radiation	Downward longwave radiation	Net radiation
Farouki scheme			
r	0.223	0.959	0.492
Bias (W m^{-2})	-5.478	9.272	26.585
SEE (W m^{-2})	23.733	14.303	76.338
JN scheme			
r	0.227	0.959	0.492
Bias (W m^{-2})	-5.406	8.523	25.764
SEE (W m^{-2})	23.698	13.839	76.222
LN scheme			
r	0.228	0.959	0.491
Bias (W m^{-2})	-5.043	8.865	25.743
SEE (W m^{-2})	23.693	14.041	76.215

Fig. 4 Observed and simulated soil temperature (°C) at different depths at the NMQ site from 1 November 2010 to 31 May 2012

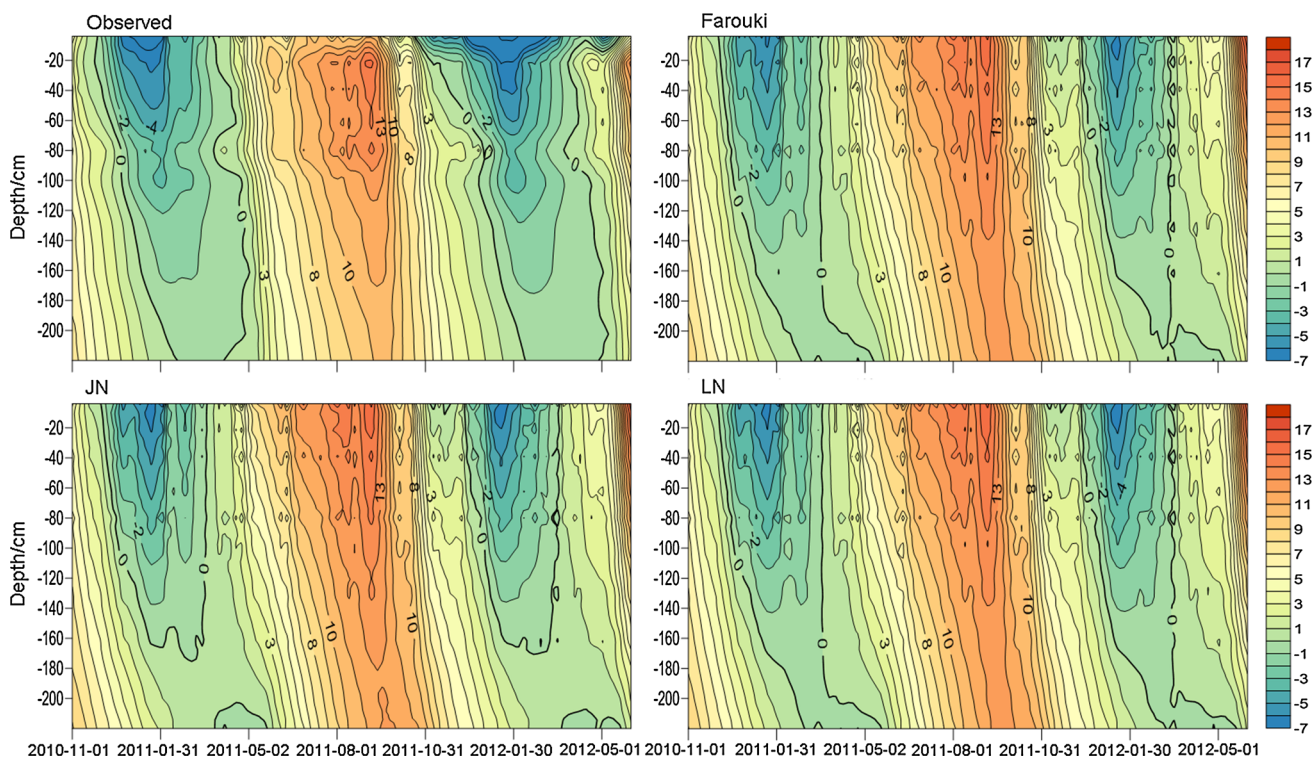


compared with the observations. However, they distinctly overestimate the soil temperature at a 4 cm depth, particularly after May 2011; therefore, the upward longwave radiation is overestimated; the cause of this result requires further study. Generally, the three schemes simulate the soil temperature higher than the observations. The Farouki scheme soil temperature at an 80 cm depth is the best, with a bias of 0.149 °C (Table 4). After modifying the soil conductivity parameterization scheme, the JN and LN scheme soil temperatures at 4 and 20 cm depths are not significantly improved. Although the correlation

confidences with the observed data are enhanced, the SEE decreased and the Bias increased. The soil temperature below a 100 cm depth as simulated by the JN and LN schemes is more similar to the observed data. The LN scheme soil temperature at a depth of 160 cm is much closer to the observed data than the other two schemes. However, below the depth of 160 cm, the soil temperatures simulated by the LN scheme and, particularly, by the JN scheme are higher than those simulated by the Farouki scheme. However, it is worth noting that the modified schemes (JN and LN) improve the simulation of the soil

Table 4 Statistical values of the three schemes' simulated and observed soil temperatures

Soil depth (cm)	Farouki scheme			JN scheme			LN scheme		
	Bias (°C)	SEE (°C)	<i>r</i>	Bias (°C)	SEE (°C)	<i>r</i>	Bias (°C)	SEE (°C)	<i>r</i>
4	4.247	5.089	0.916	4.007	4.867	0.918	4.125	4.983	0.917
20	1.234	1.575	0.989	1.017	1.393	0.990	1.114	1.462	0.990
40	1.360	1.724	0.985	1.173	1.549	0.986	1.244	1.613	0.986
60	1.169	1.644	0.979	1.010	1.488	0.981	1.056	1.542	0.980
80	0.149	1.231	0.973	0.019	1.164	0.975	0.040	1.204	0.974
100	1.220	1.600	0.978	1.119	1.474	0.981	1.115	1.497	0.980
130	0.922	1.299	0.981	0.865	1.179	0.983	0.822	1.198	0.982
160	0.966	1.209	0.987	0.952	1.225	0.982	0.871	1.154	0.985
200	0.812	1.205	0.985	0.856	1.353	0.968	0.725	1.230	0.978
220	0.771	1.403	0.973	0.845	1.644	0.945	0.687	1.489	0.961
Mean	1.285	1.798	0.974	1.186	1.733	0.971	1.180	1.737	0.973

**Fig. 5** The isotherms of the soil temperature simulated by the three schemes and the observations from 1 November 2010 to 31 May 2012

temperature. For example, their correlation confidences with the observed data increased, and the SEE and Bias with the observed data decreased, particularly for the LN scheme. Overall, the soil temperature simulated by the LN scheme is most similar to the observed data; the correlation coefficient is 0.973, the Bias is 1.180 °C and the SEE is 1.737 °C.

Figure 5 shows the isotherms of the soil temperature simulated by the three schemes and observed data from

November 2010 to May 2012. The start date of the soil freezing process is defined as when the daily mean soil temperature becomes successively negative. The observed surface soil began to freeze on 29 November 2010 and 22 October 2012. The Farouki scheme's simulated surface soil began to freeze on 1 December 2010 and 6 November 2012. For the JN scheme, the surface soil began to freeze on 1 December 2010 and 11 December 2012. For the LN scheme, the surface soil began to freeze on 1 December

Table 5 Days (d) of simulated and observed soil thawing and freezing from 1 November 2010 to 31 May 2012 (total of 577)

	4 cm	20 cm	40 cm	60 cm	80 cm	100 cm	130 cm	160 cm	200 cm	220 cm
Observed	243/334	314/263	306/271	330/247	404/173	331/246	354/223	355/222	399/178	452/125
Farouki scheme	369/208	380/197	389/188	401/156	408/149	419/158	435/142	457/120	500/77	452/125
JN scheme	356/221	370/207	380/197	394/183	406/151	421/156	454/103	504/73	571/6	474/103
LN scheme	358/219	370/207	380/197	393/184	400/157	411/146	433/144	453/124	512/65	446/131

2010 and 12 December 2012. Thus, the three schemes delay the start of the surface soil freezing compared with the observations. The start date of the soil thawing process is defined as when the daily mean soil temperature becomes successively positive. The observed data show that the surface soil began to thaw on 31 March 2010 and 20 May 2012. The Farouki scheme surface soil began to thaw on 13 March 2010 and 18 March 2012. For the JN scheme, the surface soil began to thaw on 22 March 2010 and 19 March 2012. For the LN scheme, the soil began to thaw on 22 March 2010 and 18 March 2012. Thus, the simulated start dates of the soil thawing are earlier than the observations.

Meanwhile, the three schemes simulated and observed days of soil thawing (when the daily mean soil temperature is consistently greater than 0 °C) and freezing (when the daily mean soil temperature is consistently less than 0 °C) are listed in Table 5. As seen in the table, except for the depths of 80 and 220 cm, the number of soil thawing days simulated by the three schemes is obviously higher than that for the observations; the opposite is true for the soil freezing days. The Farouki scheme’s soil freezing and thawing days at a 220 cm depth are the same as the observations. At an 80 cm depth, all of the schemes simulated the soil freezing and thawing days near the observed values. In the shallow layer of 4–60 cm, no large differences exist among the three schemes. However, below a 100 cm depth, the soil freezing and thawing days simulated by the LN scheme approach the observed value, as expected from Table 4.

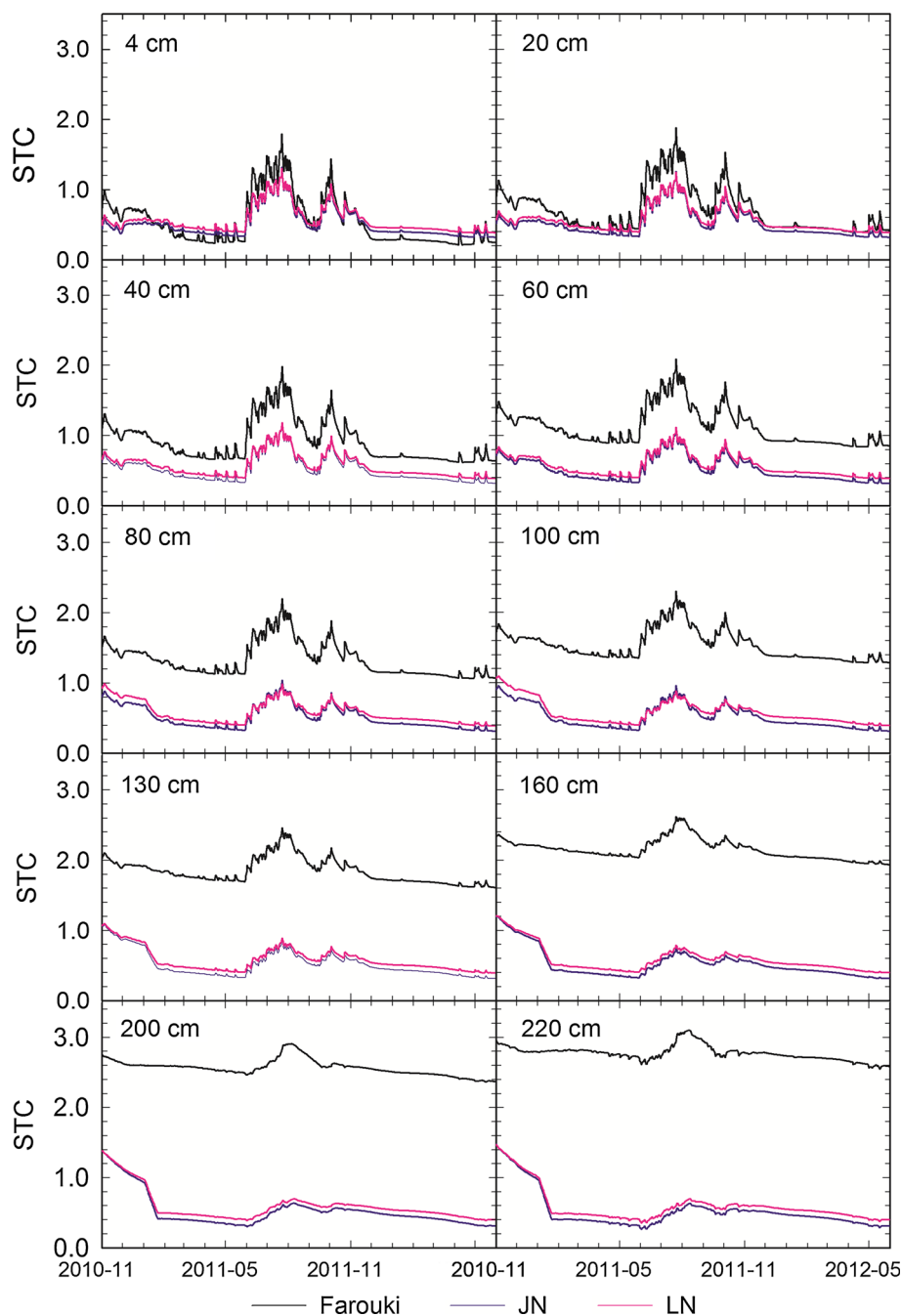
The 0 °C isotherm patterns of the observed data, the Farouki scheme and the LN scheme are similar (Fig. 5). The observed data show that freezing and thawing processes are rapid from the surface to a depth of 220 cm, with the deepest freezing depth below 220 cm. For the JN scheme, the soil freezing and thawing processes are evidently faster, with a maximum freezing depth (cold tongue) of approximately 175 cm. An unfrozen layer exists between the depths of 175 and 200 cm. Moreover, the observed data indicate that freezing and thawing proceed from the upper layers to the lower layers. However, for the Farouki and LN schemes, the soil thawing process practically proceeds simultaneously from the upper layers to a depth of approximately 160 cm, while the soil

thawing below that depth is gradual and successive. The simulated soil temperature above 60 cm is higher than the observed soil temperature during the freezing period; thus, the downward heat flux transfer is accelerated, which results in rapid soil thawing and a short freezing period.

Soil thermal conductivity

From Table 2, we see that the soil solids’ thermal conductivity values of the Farouki scheme are very large, with an average value of 8.46 W m⁻¹ K⁻¹. The average value of the soil solids’ thermal conductivity of the Johansen scheme is 3.54 W m⁻¹ K⁻¹. Figure 6 shows the temporal variation in the daily mean soil thermal conductivity of the three schemes. Because of the lack of soil thermal conductivity observations, we are unable to qualitatively or quantitatively evaluate the simulated soil thermal conductivity; instead, we simply analyze the simulated results. The soil thermal conductivity is low and relatively stable in the completely frozen stage but high and variable in the completely thawed stage. The soil thermal conductivity below a depth of 100 cm is larger when soil freezing occurs (ice and liquid coexist) than at other times. The simulated soil thermal conductivity increases as the soil depth increases overall. The sand had higher values of thermal conductivity than the clay loam (Abu-Hamdeh and Reeder 2000). The simulation by Luo et al. (2009b) suggested that a higher percent of sand (Table 2) will produce high soil thermal conductivities. At the shallow depths of 4 and 20 cm, no large differences occur among the three schemes’ soil thermal conductivities. However, at deep depths, the soil thermal conductivity values of the Farouki scheme are distinctly high. The soil thermal conductivity values of the Farouki scheme are highest during the entire simulation period. The soil thermal conductivity values of the other two schemes are relatively similar, and the JN scheme has the lowest values. Therefore, the low soil thermal conductivity values of JN may be unable to transfer the soil heat in the shallow layers to the deeper layers. This situation leads to a small “cold tongue”. The soil thermal conductivity values of the Farouki and LN schemes are high when the soil begins to thaw; as a result, large “warm tongues” occur.

Fig. 6 Simulated soil thermal conductivity ($\text{W m}^{-1} \text{K}^{-1}$) at different depths at the NMQ site from 1 November 2010 to 31 May 2012

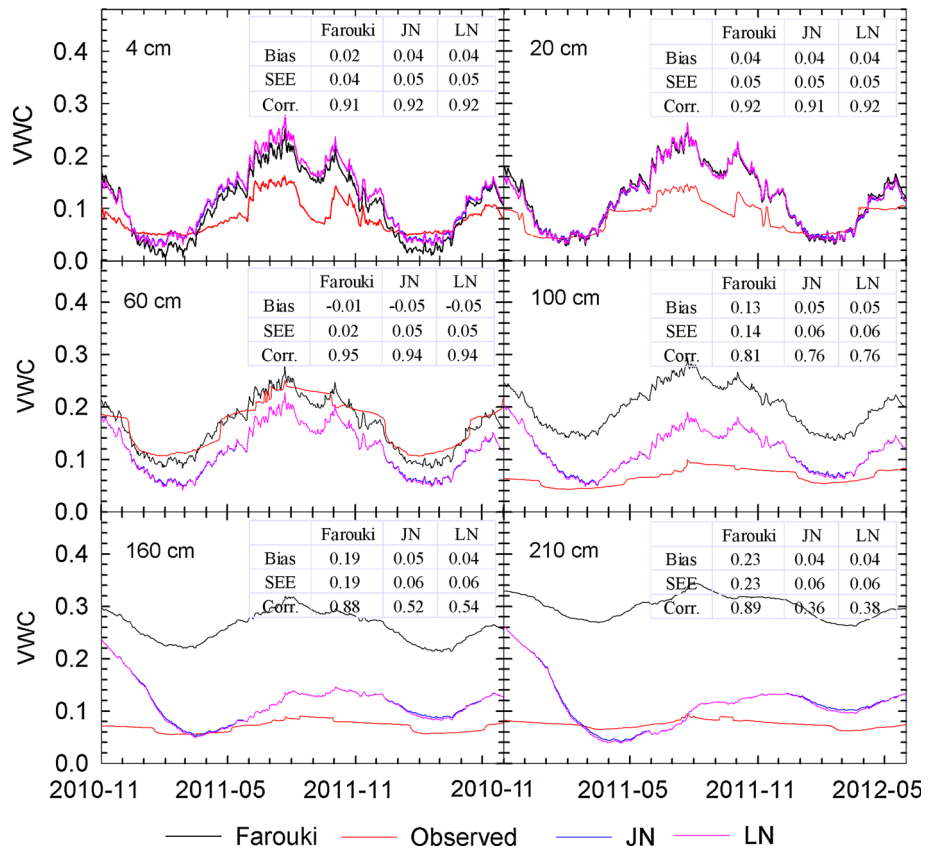


Soil water content

Figure 7 displays the observed and simulated daily mean soil volumetric water content variations from 1 November 2010 to 31 May 2012. The observed data show that the soil volumetric water content decreases as the soil begins to freeze and increases as the soil begins to thaw. Meanwhile, the shallow-layer soil water contents are significantly affected by precipitation (Fig. 2), evaporation and infiltration in the soil thawing stage. The soil water content at a

60 cm depth is the highest, with an average value of $0.166 \text{ m}^3 \text{ m}^{-3}$. The trends and values of the soil volumetric water content below a 60 cm depth are largely consistent. Previous studies suggested that groundwater influences the soil moisture, thereby influencing the surface energy and water balances in regions where the water table is shallow (Chen and Hu 2004; Yeh and Eltahir 2005; Gayler et al. 2013). Higher soil water content below a 100 cm depth as simulated by the original scheme (the Farouki scheme) is the result of not considering the water exchange between

Fig. 7 Same as Fig. 4, but for soil volumetric water content ($\text{m}^3 \text{m}^{-3}$)



the soil column and its underlying aquifer. The simulated soil water contents of the three schemes at the shallow layers of 4 and 20 cm are relatively good but slightly lower during soil freezing and higher during soil thawing. The simulation ability of the Farouki scheme for soil water content is best at a 60 cm depth, with a small negative bias of $0.01 \text{ m}^3 \text{ m}^{-3}$. The study of Luo et al. (2009b) indicated that the differences in the soil thermal conductivity of the Farouki, JN, and LN schemes are large when the soil water content is low but small when the soil water content is high. Therefore, the differences in the soil thermal conductivity among the schemes are small in the upper layers but large in the deep layers (Fig. 6). Yang et al. (2003) suggested that soil freezing and thawing processes are strongly influenced by the soil water content. Because water has the largest heat capacity among all materials, latent heat is released in the process of the freezing phase change, while heat is absorbed in the process of the thawing phase change. Below the depth of 100 cm, the simulated soil volumetric water content is higher. After modifying the groundwater parameterizations (the JN and LN schemes), the soil volumetric water content is higher than the observed data, except at 60 and 210 cm depths, when the soil begins to freeze or thaw, which delays/advances the soil freezing/thawing. In spite of the fact that the correlation coefficients between the simulated soil

water content and observed data decreased, their biases and standard errors greatly decreased, which means that the simulated values are close to the observed data. In general, biases and standard errors between the LN scheme and observed data are the smallest, with average values of 0.026 and $0.054 \text{ m}^3 \text{ m}^{-3}$.

Concluding remarks

This paper compared simulated results (radiation components, soil temperature, soil freezing and thawing processes, soil water content and thermal conductivity) of the original water-heat parameterization scheme (the Farouki scheme) and modified soil water-heat parameterization schemes (the JN and LN schemes) in CLM3.5 using the same atmospheric forcing data observed at NMQ in the Central Tibetan Plateau with observations. The major findings are as follows:

Compared with the observed and Farouki-scheme-simulated radiation components, the JN scheme improves the simulation of upward longwave radiation, and the LN scheme improves the simulation of upward shortwave radiation and net radiation. The soil temperatures in 10 layers are higher for the three schemes than for the observed data. However, the modified schemes,

particularly the LN scheme, improve the simulated soil temperature effects. The soil thawing/freezing days are overestimated/underestimated by the three schemes. The JN scheme soil freezing and thawing processes are more rapid, and the “cold tongue” is smaller than that of the observed data. The observed freezing and thawing proceed from the upper layers to the lower layers, while for the Farouki and LN schemes, the soil thawing proceeds simultaneously from the upper layers to a depth of approximately 160 cm; the soil thawing below the depth of 160 cm proceeds successively and slowly. Specifically, at the shallow layers of 4 and 20 cm, no large differences occur among the three schemes’ soil thermal conductivities. However, at deeper depths, the soil thermal conductivity values of the Farouki scheme are distinctly large. The soil thermal conductivity values of the Farouki scheme are the highest during the entire simulation period. Higher soil water contents below 100 cm are simulated by the Farouki scheme. The modeling of the soil water content can be improved, particularly for LN scheme, through implementing water exchange between the soil column and its underlying aquifer.

Although the modified schemes’ soil temperatures and water contents in particular layers are coherent with the observed results in this paper, the simulations were conducted for a single point and the simulation period and spin-up time were short. In addition, because of the sparse observations of soil-ice content, sensible and latent heat fluxes, surface soil heat flux, and soil thermal conductivity, our results require further verification. Overall, the simulated soil water contents are generally higher than the observed values; as a result, the soil thermal capacity and soil temperatures are likely to be higher. These conditions have a significant impact on the processes of soil freezing and thawing. Therefore, the parameterizations of soil water–heat interactions need improvement.

Acknowledgments This work was supported by the Innovation Research Group of NSFC (41121001), the ‘Strategic Priority Research Program (B)’ of CAS (XDB03030204), the State Key Laboratory of Cryospheric Sciences (SKLCS-ZZ-2013-02-07), CAREERI, CAS, the International Innovative Group Project of CAS (Y42AC71001), the National Natural Science Foundation of China (41075007), and the National Key Basic Research Program of China (2010CB951404). The authors thank the Supercomputing Center, CAREERI, CAS, for their help of model simulations. We are grateful to Dr. Guoyue Niu and Mingxing Li for providing their groundwater codes. We are also indebted to the reviewers for helpful comments and criticisms of the initial draft of this paper.

References

- Abu-Hamdeh NH, Reeder RC (2000) Soil thermal conductivity effects of density, moisture, salt concentration, and organic matter. *Soil Sci Soc Am J* 64:1285–1290
- Chen X, Hu Q (2004) Groundwater influences on soil moisture and surface evaporation. *J Hydrol* 297:285–300
- Chen BL, Lü SH, Luo SQ (2013a) Simulation analysis on land surface process at Maqu station in the Qinghai-Xizang Plateau using Community Land Model. *Plat Meteorol* 31:1511–1522 (in Chinese with English Abstract)
- Chen XL, Yang MX, Wan GN, Wang XJ (2013b) Simulation studies of CLM3 and SHAW at NMQ station on the central Tibetan Plateau. *J Glaciol Geocryol* 35:291–300 (in Chinese with English Abstract)
- Cherkauer KA, Lettenmaier DP (1999) Hydrologic effects of frozen soils in the upper Mississippi River Basin. *J Geophys Res* 104:19599–19610
- Clapp RB, Hornberger GM (1978) Empirical equations for some soil hydraulic properties. *Water Resour Res* 14:601–604
- Collins WD, Bitz CM, Blackmon ML, Bonan GB, Bretherton CS, Carton JA, Chang P, Doney SC, Hack JJ, Henderson TB, Kiehl JT, Large WG, McKenna DS, Santer BD, Smith RD (2006) The Community Climate System Model: CCSM3. *J Clim* 19:2122–2143
- Côté J, Konrad JM (2005) A generalized thermal conductivity model for soils and construction materials. *Can Geotech J* 42:443–458
- Davin EL, Stöckli R, Jaeger EB, Levis S, Seneviratne SI (2011) COSMO-CLM2: a new version of the COSMO-CLM model coupled to the Community Land Model. *Clim Dyn* 37:1889–1907
- Dickinson RE, Henderson-Sellers A, Kennedy PJ (1993) Biosphere–Atmosphere Transfer Scheme (BATS) Version 1e as Coupled to the NCAR Community Climate Model. NCAR/TN-387 + STR
- Farouki OT (1981) Thermal properties of soil. USA Cold Regions Research and Engineering Laboratory, CRREL Monograph 81-1
- Gayler S, Ingwersen J, Priesack E, Wöhling T, Wulfmeyer V, Streck T (2013) Assessing the relevance of subsurface processes for the simulation of evapotranspiration and soil moisture dynamics with CLM3.5: comparison with field data and crop model simulations. *Environ Earth Sci* 69:415–427. doi:10.1007/s12665-013-2309-z
- Giorgi F, Coppola E, Solmon F, Mariotti L, Sylla MB, Bi X, Elguindi N, Diro GT, Nair V, Giuliani G, Turuncoglu UU, Cozzini S, Guttler I, O’Brien TA, Tawfik AB, Shalaby A, Zakey AS, Steiner AL, Stordal F, Sloan LC, Brankovic C (2012) RegCM4: model description and preliminary tests over multiple CORDEX domains. *Clim Res* 52:7–29
- Guo DL, Wang HJ (2013) Simulation of permafrost and seasonally frozen ground conditions on the Tibetan Plateau, 1981–2010. *J Geophys Res* 118:5216–5230
- Guo DL, Yang MX, Wang HJ (2010) Sensible and latent heat flux response to diurnal variation in soil surface temperature and moisture under different freeze/thaw soil conditions in the seasonal frozen soil region of the central Tibetan Plateau. *Environ Earth Sci* 63:97–107. doi:10.1007/s12665-010-0672-6
- Johansen O (1977) Thermal conductivity of soils. PhD thesis, University of Trondheim, Norway
- Koren V, Schaake J, Mitchell K, Duan QY, Chen F, Baker JM (1999) A parameterization of snowpack and frozen ground intended for NCEP weather and climate models. *J Geophys Res* 104:19569–19585
- Lawrence PJ, Chase TN (2007) Representing a new MODIS consistent land surface in the Community Land Model (CLM 3.0). *J Geophys Res* 112:G01023. doi:10.1029/2006JG000168
- Li X, Koike T (2003) Frozen soil parameterization in SiB2 and its validation with GAME-Tibet observations. *Cold Reg Sci Tech* 36:165–182. doi:10.1016/S0165-232X(03)00009-0
- Luo SQ, Lü SH, Zhang Y (2009a) Development and validation of the frozen soil parameterization scheme in Common Land Model.

- Cold Reg Sci Tech 55:130–140. doi:[10.1016/j.coldregions.2008.07.009](https://doi.org/10.1016/j.coldregions.2008.07.009)
- Luo SQ, Lü SH, Zhang Y, Hu ZY, Ma YM, Li SS, Shang LY (2009b) Soil thermal conductivity parameterization establishment and application in numerical model of central Tibetan Plateau. *Chin J Geophys* 52:919–928 (in Chinese with English Abstract)
- Ma YM, Wang Y, Wu R, Hu Z, Yang K, Li M, Ma W, Zhong L, Sun F, Chen X, Zhu Z, Wang S, Ishikawa H (2009) Recent advances on the study of atmosphere-land interaction observations on the Tibetan Plateau. *Hydrolo Earth Syst Sci* 13:1103–1111
- Niu GY, Yang ZL (2006) Effects of frozen soil on snowmelt runoff and soil water storage at a continental scale. *J Hydrometeorol* 7:937–952
- Niu GY, Yang ZL, Dickinson RE, Gulden LE (2005) A simple TOPMODEL-based runoff parameterization (SIMTOP) for use in global climate models. *J Geophys Res* 110:D21106. doi:[10.1029/2005JD006111](https://doi.org/10.1029/2005JD006111)
- Niu GY, Yang ZL, Dickinson RE, Gulden LE, Su H (2007) Development of a simple groundwater model for use in climate models and evaluation with Gravity Recovery and Climate Experiment data. *J Geophys Res* 112:D07103. doi:[10.1029/2006JD007522](https://doi.org/10.1029/2006JD007522)
- Niu GY, Yang ZL, Mitchell KE, Chen F, Ek MB, Barlage M, Kumar A, Manning K, Niyogi D, Rosero E, Tewari M, Xia YL (2011) The community Noah land surface model with multiparameterization options (Noah-MP): 1. Model description and evaluation with local-scale measurements. *J Geophys Res* 116:D12109. doi:[10.1029/2010JD015139](https://doi.org/10.1029/2010JD015139)
- Oleson K, Lawrence DM, Bonan GB et al (2013) Technical description of version 4.5 of the Community Land Model (CLM). NCAR Technical Note NCAR/TN-503 + STR. doi:[10.5065/D6RR1W7M](https://doi.org/10.5065/D6RR1W7M)
- Oleson KW, Dai YJ, Bonan G, Bosilovich M, Dickinson R, Dirmeyer P, Hoffman F, Houser P, Levis S, Niu GY, Thornton E, Vertenstein M, Yang ZL, Zeng XB (2004) Technical description of the Community Land Model (CLM). NCAR Technical Note NCAR/TN-461 + STR
- Peters-Lidard CD, Blackburn E, Liang X, Wood EF (1998) The effect of soil thermal conductivity parameterization on surface energy fluxes and temperatures. *J Atmos Sci* 55:1209–1224
- Rangarajan S (1963) Thermal effects of the Tibetan Plateau during the Asian monsoon season. *Aust Meteorol Mag* 42:24–34
- Rockel B, Will A, Hense A (2008) The regional climate model COSMO-CLM (CCLM). *Meteorol Z* 17:347–348
- Sellers PJ, Mintz Y, Sad YC, Dalcher A (1986) A simple biosphere model (SIB) for use within general circulation models. *J Atmos Sci* 43:505–531
- Sellers PJ, Randall DA, Collatz GJ, Berry JA, Field CB, Dazlich DA, Zhang C, Collelo GD, Bounoua L (1996) A revised land surface parameterization (SiB2) for atmospheric GCMs: Part I. Model formulation. *J Clim* 9:676–705
- Slater AG, Pitman AJ, Desborough CE (1998) Simulation of freeze-thaw cycles in a circulation model land surface scheme. *J Geophys Res* 103:11303–11312
- Smirnova TG, Brown JM, Benjamin SG, Kim D (2000) Parameterization of cold-season processes in the MAPS land-surface scheme. *J Geophys Res* 105:4077–4086
- Takata K, Kimoto M (2000) A numerical study on the impact of soil freezing on the Continental-scale seasonal cycle. *J Meteorol Soc Jpn* 78:199–221
- Thornton PE, Zimmermann NE (2007) An improved canopy integration scheme for a land surface model with prognostic canopy structure. *J Clim* 20:3902–3923
- Wang CH, Dong WJ, Wei ZG (2003) Study on relationship between the frozen-thaw process in Qinghai-Xizang Plateau and circulation in east-Asia. *Chin J Geophys* 46:310–316 (in Chinese with English Abstract)
- Wang XJ, Yang MX, Wan GN, Chen XL, Pang GJ (2013) Qinghai-Xizang (Tibetan) Plateau climate simulation using the regional climate model RegCM3. *Clim Res* 57:173–186
- Wu GX, Liu YM, He B, Bao Q, Duan A, Jin FF (2012) Thermal controls on the Asian summer monsoon. *Sci Rep* 2:404. doi:[10.1038/srep00404](https://doi.org/10.1038/srep00404)
- Xia K, Luo Y, Li WP (2011) Simulation of freezing and melting of soil on the northeast Tibetan Plateau. *Chin Sci Bull* 56:2145–2155. doi:[10.1007/s11434-011-4542-8](https://doi.org/10.1007/s11434-011-4542-8)
- Xiao Y, Zhao L, Dai YJ, Li R, Pang QQ, Yao JM (2012) Representing permafrost properties in CoLM for the Qinghai-Xizang (Tibetan) Plateau. *Cold Reg Sci Tech* 87:68–77. doi:[10.1016/j.coldregions.2012.12.004](https://doi.org/10.1016/j.coldregions.2012.12.004)
- Xu L, Dirmeyer P (2011) Snow-atmosphere coupling strength in a global atmospheric model. *Geophys Res Lett* 38:L13401. doi:[10.1029/2011GL048049](https://doi.org/10.1029/2011GL048049)
- Xu XD, Lu CG, Shi XH, Gao ST (2008) World water tower: an atmospheric perspective. *Geophys Res Lett* 35:L20815. doi:[10.1029/2008GL035867](https://doi.org/10.1029/2008GL035867)
- Yang MX, Yao TD, Gou XH, Koike T, He YQ (2003) The soil moisture distribution, thawing-freezing processes and their effects on the seasonal transition on the Qinghai-Xizang (Tibetan) plateau. *J Asian Earth Sci* 21:457–465
- Yang MX, Yao TD, Gou XH, Tang HG (2007) Water recycling between the land surface and atmosphere on the Northern Tibetan Plateau—a case study at flat observation sites. *Arct Antarct Alp Res* 39:694–698
- Yang K, Chen YY, Qin J (2009) Some practical notes on the land surface modeling in the Tibetan Plateau. *Hydro Earth Syst Sci* 13:687–701
- Yang MX, Nelson FE, Shiklomanov NI, Guo DL, Wan GN (2010) Permafrost degradation and its environmental effects on the Tibetan Plateau: a review of recent research. *Earth Sci Rev* 103:31–44
- Yang K, Wu H, Qin J, Lin CG, Tang WJ, Chen YY (2014) Recent climate changes over the Tibetan Plateau and their impacts on energy and water cycle: a review. *Glob Planet Change* 112:79–91
- Yao TD, Thompson L, Yang W, Yu WS, Gao Y, Guo XJ, Yang XX, Duan K, Zhao HB, Xu BQ, Pu JC, Lu AX, Xiang Y, Kattel DB, Joswiak D (2012) Different glacier status with atmospheric circulations in Tibetan Plateau and surroundings. *Nat Clim Change* 2:663–667
- Ye DZ, Gao YX (1979) The meteorology of the Qinghai-Xizang (Tibet) Plateau. Science Press, Beijing, pp 30–55 (in Chinese)
- Yeh PJF, Eltahir EAB (2005) Representation of water table dynamics in a land surface scheme. Part I: model development. *J Clim* 18:1861–1880. doi:[10.1175/JCLI3330.1](https://doi.org/10.1175/JCLI3330.1)
- Yi S, Chen J, Wu Q, Ding Y (2013) Simulating the role of gravel on the dynamics of permafrost on the Qinghai-Tibetan Plateau. *Cryosphere Disc* 7:4703–4740
- Zhang Y, Lü SH (2002) Development and validation of a simple frozen soil parameterization scheme used for climate model. *Adv Atmos Sci* 19:513–527
- Zhang T, Nelson FE, Gruber S (2007a) Introduction to special section: permafrost and seasonally frozen ground under a changing climate. *J Geophys Res* 112:F02S01. doi:[10.1029/2007JF000821](https://doi.org/10.1029/2007JF000821)
- Zhang X, Sun SF, Xue Y (2007b) Development and testing of a frozen soil parameterization for cold region studies. *J Hydrometeorol* 8:690–701